RESEARCH ARTICLE

Yeast WILEY

Comparison of Xrn1 and Rat1 5′ → 3′ exoribonucleases in budding yeast supports the specific role of Xrn1 in cotranslational mRNA decay

José E. Pérez-Ortín[1,2] | Antonio Jordán-Pla[1] | Yujie Zhang[2] |
Jorge Moreno-García[1] | Claudio Bassot[3] | Marina Barba-Aliaga[1] |
Leire de Campos-Mata[4] | Mordechai Choder[5] | Juana Díez[4] | Ilaria Piazza[3] |
Vicent Pelechano[2] | José García-Martínez[1]

[1]Instituto de Biotecnología y Biomedicina (BIOTECMED), Facultad de Biológicas, Universitat de València, Burjassot, Spain

[2]SciLifeLab, Department of Microbiology, Tumor and Cell Biology, Karolinska Institutet, Solna, Sweden

[3]Max Delbrück Center for Molecular Medicine in the Helmholtz Association (MDC Berlin), Berlin, Germany

[4]Virology Unit, Department of Experimental and Health Sciences, Universitat Pompeu Fabra, Barcelona, Spain

[5]Department of Molecular Microbiology, Technion-Israel Institute of Technology, Rappaport Faculty of Medicine, Haifa, Israel

Correspondence
José E. Pérez-Ortín and José García-Martínez, Departamento de Bioquímica y Biología Molecular Facultad de Biológicas. Universitat de València. C/Dr. Moliner 50. E46100 Burjassot, Spain.
Email: jose.e.perez@uv.es and jose.garcia-martinez@uv.es

Vicent Pelechano, SciLifeLab, Department of Microbiology, Tumor and Cell Biology, Karolinska Institutet, 17165 Solna, Swede.
Email: vicent.pelechano@scilifelab.se

Present addresses
Antonio Jordán-Pla, Developmental Neurobiology Unit, Instituto de Biomedicina de Valencia IBV-CSIC, Valencia, Spain.

Leire de Campos-Mata, Department of Medical Biochemistry and Biophysics, Division of Immunology, Karolinska Institutet, Stockholm, Sweden.

Funding information
Spanish MCIN/AEI/10.13039/501100011033, Grant/Award Number: PID2020-112853GB-C31; Swedish Foundation's Starting Grant; Swedish Research Council, Grant/Award Numbers: VR 2020-01480, 2021-06112, 2019-02335, 2018-05973; Wallenberg Academy Fellowship,

Abstract

The yeast *Saccharomyces cerevisiae* and most eukaryotes carry two 5′ → 3′ exoribonuclease paralogs. In yeast, they are called Xrn1, which shuttles between the nucleus and the cytoplasm, and executes major cytoplasmic messenger RNA (mRNA) decay, and Rat1, which carries a strong nuclear localization sequence (NLS) and localizes to the nucleus. Xrn1 is 30% identical to Rat1 but has an extra ~500 amino acids C-terminal extension. In the cytoplasm, Xrn1 can degrade decapped mRNAs during the last round of translation by ribosomes, a process referred to as "cotranslational mRNA decay." The division of labor between the two enzymes is still enigmatic and serves as a paradigm for the subfunctionalization of many other paralogs. Here we show that Rat1 is capable of functioning in cytoplasmic mRNA decay, provided that Rat1 remains cytoplasmic due to its NLS disruption (cRat1). This indicates that the physical segregation of the two paralogs plays roles in their specific functions. However, reversing segregation is not sufficient to fully complement the Xrn1 function. Specifically, cRat1 can partially restore the cell volume, mRNA stability, the proliferation rate, and 5′ → 3′ decay alterations that characterize *xrn1Δ* cells. Nevertheless, cotranslational decay is only slightly complemented by cRat1. The use of the *AlphaFold* prediction for cRat1 and its subsequent docking with the ribosome complex and the sequence conservation between cRat1 and Xrn1 suggest that the tight interaction with the ribosome

observed for Xrn1 is not maintained in cRat1. Adding the Xrn1 C-terminal domain to
Rat1 does not improve phenotypes, which indicates that lack of the C-terminal is not
responsible for partial complementation. Overall, during evolution, it appears that
the two paralogs have acquired specific characteristics to make functional
partitioning beneficial.

KEYWORDS

C-terminal domain, exoribonuclease, Frame Protection Index (FPI), mRNA decay,
Saccharomyces cerevisiae, synthesis rate

1 | INTRODUCTION

In eukaryotes, $5' \rightarrow 3'$ decay plays a crucial role in controlling RNA
processing, quality, and quantity. $5' \rightarrow 3'$ exoribonucleases (XRNs) are
conserved across eukaryotes and play crucial roles in the processing
and degradation of messenger RNA (mRNA) and noncoding (nc) RNA.
XRNs recognize RNAs with a $5'$-monophosphate ($5'$P) end that arises
from endonucleolytic or exonucleolytic cleavage or decapping, and
trim RNA processively in the $5' \rightarrow 3'$ direction (Chang et al., 2011;
Nagarajan et al., 2013). The molecular functions of XRNs have been
studied mostly in the budding yeast *Saccharomyces cerevisiae*, which
possesses two XRNs: cytoplasmic XRN, Xrn1, and a nuclear XRN, Xrn2
(also referred to as Rat1) (Amberg et al., 1992; Heyer et al., 1995;
Johnson, 1997). In yeast, Xrn1 is responsible for a cytoplasmic
deadenylation-dependent mRNA $5' \rightarrow 3'$ exonucleolytic decay
(Nagarajan et al., 2013; Parker & Song, 2004). Indeed, the demon-
strated activity as $5' \rightarrow 3'$ XRN (Larimer & Stevens, 1990; Larimer
et al., 1992) is the reason for its Xrn1 name. Xrn1 $5' \rightarrow 3'$
exonucleolytic activity on mRNAs is fundamental for the decay of
both correct and defective molecules, provided that they have a $5'$P
end caused by either decapping or endonucleolytic cleavage
(Nagarajan et al., 2013; Parker & Song, 2004). Xrn1p can also
hydrolyze NAD-capped mRNAs (deNADase activity) and then exonu-
cleolytically degrade them processively (Sharma et al., 2022). Its
enzymatic activity can even act cotranslationally on ribosome-
associated mRNAs. In this context, Xrn1 trails the last translating
ribosome (Pelechano et al., 2015) with which it specifically interacts
physically (Tesina et al., 2019). Xrn1 plays additional roles in mRNA
processing and quality control, ribosomal RNA (rRNA) processing,
transfer RNA quality, and ncRNA decay (Langeberg et al., 2020;
Nagarajan et al., 2013; Parker & Song, 2004; Sharma et al., 2022).
Apart from its RNA decay activities, Xrn1 is associated with
microtubules (Interthal et al., 1995) and microtubule-related processes,
such as meiosis (Solinger et al., 1999) and conjugation (Kar-enhancing
mutation: KEM1 = XRN1; Kim et al., 1990).

Both $5' \rightarrow 3'$ XRNs are partially homologous (Kenna et al., 1993;
Nagarajan et al., 2013) and have been shown to be functionally
interchangeable, although they are thought to be restricted to
specific cellular compartments: Xrn1 in the cytoplasm and Rat1 in the
nucleus (Johnson, 1997). *RAT1* is an essential gene, whereas *XRN1* is

> **Take-away**
>
> - Cytoplasmic Rat1 partly restores the general physiologi-
>   cal defects of an *xrn1Δ* mutant.
> - cRat1 is very inefficient in cotranslational mRNA decay.
> - The C-terminal domain of Xrn1 is not involved in $5' \rightarrow 3'$
>   cotranslational decay.

not (Johnson, 1997). The ectopic nuclear localization of Xrn1 by the
addition of an SV40 nuclear location sequence (NLS) can rescue *rat1*
lethality, whereas cytoplasmic Rat1, which lacks its NLS, can rescue
xrn1 ski2 lethality (Johnson, 1997). *SKI2* encodes a co-factor of the
$3' \rightarrow 5'$ RNA exosome, which is essential for its cytoplasmic function
(Johnson & Kolodner, 1995). The enzymatic mechanism of Rat1 is
assumed to be processive and similar to that of Xrn1, because it
shares the active site and shows extensive conservation around it
(Basu et al., 2021; Nagarajan et al., 2013). Rat1 is also a similar
deNADing enzyme to Xrn1 (Sharma et al., 2022). Rat1 performs
important nuclear activities related to RNA metabolism, including
rRNA and small nucleolar RNA processing, as well as poly-A$^+$-
dependent and -independent mRNA transcription termination (Kim
et al., 2004). The existence of both nuclear (Rat1/Xrn2 family) and
cytoplasmic (Xrn1 family) $5' \rightarrow 3'$ XRNs is common in a variety of
studied eukaryotes (Chang et al., 2011; Han et al., 2023), and
suggests that their functional interchangeability extends across
species (reviewed in Nagarajan et al., 2013).

Rat1 apparently lacks cytoplasmic functions (Johnson, 1997). For
Xrn1, it has been shown that, albeit predominantly cytoplasmic
(Haimovich et al., 2013; Johnson, 1997), it also performs important
nuclear functions, such as rRNA processing and the degradation of
defective RNAs (Nagarajan et al., 2013), by forming a complex with
Rai1 (Xiang et al., 2009). Xrn1 also acts as a general transcription
activator by forming a complex with other decay factors (Haimovich
et al., 2013; Medina et al., 2014). The proper cytoplasmic function of
Xrn1p requires its shuttling between the cytoplasm and the nucleus
(Pérez-Ortín & Chávez, 2022), which is made possible by the recently
discovered existence of two NLSs (Chattopadhyay et al., 2022).
Budding yeast Xrn1 is a very long protein with 1528 amino acids

compared to the shorter Rat1 (1006 amino acids). The larger size of Xrn1 is due to an extended C-terminal (Cterm) segment that is absent in Rat1 (Chang et al., 2012), which is a basic, albeit nonessential, domain for most in vivo functions, and is toxic when overexpressed (Page et al., 1998). This feature, and the relatively low homology between budding yeast Xrn1 and Rat1 (30% amino acid identity), pose the question of how these two proteins can substitute one another when located in each other's cell compartment (Johnson, 1997).

In this study, our goal was to gain insight into which of the in vivo activities of Xrn1 can be substituted for Rat1. We studied two yeast strains that express *RAT1* with a defective NLS, the product of which is cytoplasmic (cRat1). We found that cRat1 partially complements many of the natural features of Xrn1, except for cotranslational decay, which is only slightly complemented by cRat1. In particular, cRat1 is not a good substitute for Xrn1, for both initiating $5' \rightarrow 3'$ decay and following the ribosome position during cotranslational mRNA decay. This failure is not improved by overexpressing cRat1 or by adding Xrn1 Cterm to cRat1, despite the fact that this construction has been previously shown to complement other differences in cRat1 activity (Blasco-Moreno et al., 2019). These results support the notion that both $5' \rightarrow 3'$ exonucleases have functionally redundant activities, but have acquired some unique features, including their cellular localization, which seem to optimize their function, and also possibly their cooperation. Our results suggest that there are other structural disparities between the two exonucleases that potentially involve distinct binding partners or the essential import of Xrn1 to the nucleus. Furthermore, the use of an *AlphaFold* model of cRat1 docked to the ribosome complex and the sequence conservation between cRat1 and Xrn1 suggest that the tight interaction with the ribosome observed for Xrn1 is not conserved in cRat1. All these features seem crucial for the full in vivo functionality of a $5' \rightarrow 3'$ XRN in co-translational mRNA decay.

2 | MATERIALS AND METHODS

2.1 | Yeast strains, plasmids, and culture conditions

Yeast cells were grown in YPD (1% yeast extract, 2% peptone, 2% glucose) or in SC-ura (synthetic complete media: 1.7 g/L yeast nitrogen base (Difco), 5 g/L (NH$_4$)$_2$SO$_4$, 20 g/L dextrose, and dropout mix [Formedium] lacking uracil to allow selection) at 30°C. Precultures were grown overnight in 250 mL flasks and shaken at 190 rpm. The next day, precultures were diluted to OD$_{600}$ = 0.05 and grown up to an OD$_{600}$ of ~0.5. For the plasmid-transformed strains, precultures were done in SC-ura and cultured the next day in YPD. Cells were recovered by centrifugation, flash-frozen in liquid nitrogen, and stored at −20°C until needed for either Genomic Run-on (GRO) or RNA extraction.

Yeast strains were transformed with centromeric plasmids YCpLac33 and pBBM3 and with multicopy 2 μm-derived plasmid pRS426 (Christianson et al., 1992) following a standard protocol (Gietz & Schiestl, 2007). Multicopy cRat1 plasmid was constructed by cloning the cRAT1 open reading frame (ORF) in the pRS426 vector. First, the cRAT1 ORF was amplified by conventional polymerase chain reaction (PCR) from plasmid pBBM3 using primers cRAT1-pRS-F: 5′-CGACGGTATCGATAAGCTTGATATCGAATTCCTGCAGCCCTG ATGAAAAACTACGAAAAGTTTAC-3′ and cRAT1-pRS-R: 5′-TCCAC CGCGGTGGCGGCCGCTCTAGAACTAGTGGATCCCCATGTTCCATT TTTTGTTATAAAATA-3′, and pBMM3 residual plasmid was destroyed by digesting with DpnI (Thermo Fisher Scientific). Then, plasmid pRS426 was linearized by SmaI (Thermo Fisher Scientific). After PCR product and plasmid purification (Thermo Fisher Scientific), the cRAT1 gene was inserted into linearized pRS426 using Gibson Assembly. Supporting Information S3: Table S1 lists both the yeast strains and plasmids.

For the generation time (GT) estimations, 50 mL of yeast cultures were grown in 250 mL flasks in either YPD or SC-ura with shaking (190 rpm) at 30°C. Aliquots were taken every 30 min in the exponential phase and their OD$_{600}$ (from 0.05 to 0.7) were measured. The GT (in minutes) in the exponential phase was calculated from growth curves (see Figure 1a and Supporting Information S1: Figure S1C–E).

The median values of cell volumes were calculated by a Coulter-Counter Z series device (Beckman Coulter). The absolute values in femtoliters (fL) are given in the legends and the relative values are shown in Figure 1 and Supporting Information S1: Figure S1.

2.2 | Reverse-transcription and quantitative PCR (RT-qPCR) analysis

For the analysis of the mRNA levels, total RNAs were isolated from yeast cells following the protocol described elsewhere (García-Martínez et al., 2004). Briefly, a volume of an exponential phase culture corresponding to 10 OD$_{600}$ units was harvested and flash-frozen. Cells were resuspended in 500 μL of cold LETS buffer (LiCl 0.1 M, EDTA pH 8.0 10 mM, Tris-HCl pH 7.4 10 mM, SDS 0.2%) and transferred to a screw-cap tube already containing 500 μL of sterile glass beads and 500 μL of acid phenol:chloroform (5:1). Then, cells were broken in the Precellys 24 tissue homogenizer (Bertin Technologies) and centrifuged. The supernatant was transferred to a new tube containing 500 μL of acid phenol:chloroform (5:1) and then to a tube containing 500 μL of chloroform:isoamyl alcohol (25:1). The RNA from the top phase was precipitated and finally dissolved in water for later quantification and quality control with a Nanodrop device (Thermo Fisher Scientific).

The RT-qPCR reactions were performed as detailed in (Garre et al., 2013). Briefly, 2.5 μg of the total DNAse-I (Roche)-treated RNA were retrotranscribed using an oligo d(T)$_{18}$ with Maxima Reverse Transcriptase (Thermo Fisher Scientific). Complementary DNA was labeled with SYBR Pre-mix Ex Taq (Tli RNase H Plus, Takara) and the Cq values were obtained from the CFX96 Touch™ Real-Time PCR Detection System (BioRad). Endogenous *RAT1* mRNA levels were determined using primers RAT1-F: 5′-GCAAGGAAGAAATTGATG
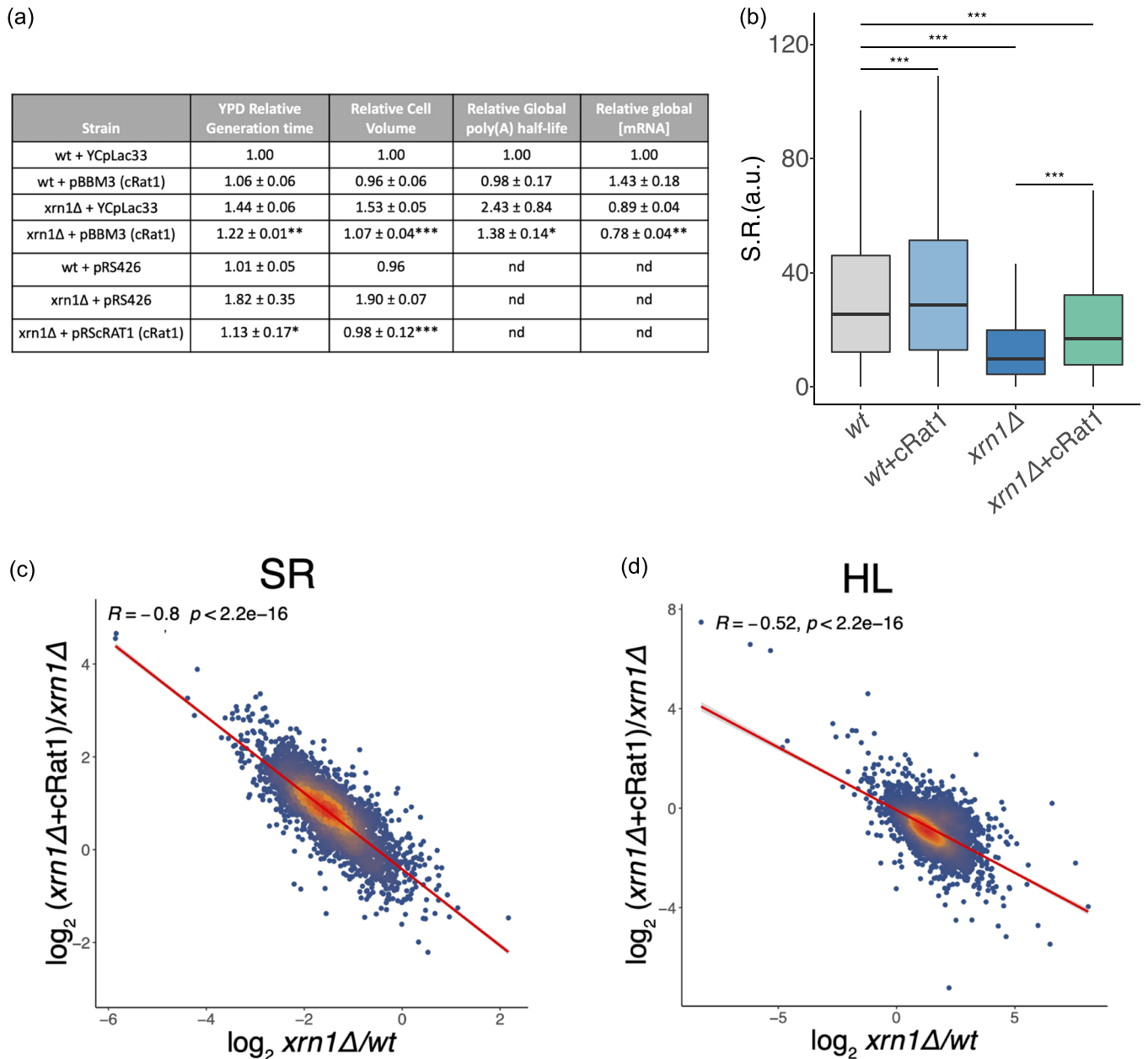
(a)

Strain	YPD Relative Generation time	Relative Cell Volume	Relative Global poly(A) half-life	Relative global [mRNA]
wt + YCpLac33	1.00	1.00	1.00	1.00
wt + pBBM3 (cRat1)	1.06 ± 0.06	0.96 ± 0.06	0.98 ± 0.17	1.43 ± 0.18
xrn1Δ + YCpLac33	1.44 ± 0.06	1.53 ± 0.05	2.43 ± 0.84	0.89 ± 0.04
xrn1Δ + pBBM3 (cRat1)	1.22 ± 0.01**	1.07 ± 0.04***	1.38 ± 0.14*	0.78 ± 0.04**
wt + pRS426	1.01 ± 0.05	0.96	nd	nd
xrn1Δ + pRS426	1.82 ± 0.35	1.90 ± 0.07	nd	nd
xrn1Δ + pRScRAT1 (cRat1)	1.13 ± 0.17*	0.98 ± 0.12***	nd	nd

FIGURE 1 The cytoplasmic version of the Rat1 protein (cRat1) restores mostly, but not totally, the main phenotypes of an *xrn1Δ* strain. (a) Generation times (GT), cell volumes, and global poly(A) messenger RNA (mRNA) stability were determined as described in the Section 2 for the studied strains grown in YPD (1% yeast extract, 2% peptone, 2% glucose). Values were relativized to those of the wild-type (WT) strain transformed with empty plasmid YCpLac33, which was taken as 1.00. As a result, the WT values lack SD and statistical comparison. The two cRat1 samples (centromeric pBBM3 and multicopy pRScRAT1), however, statistically differ from their respective *xrn1Δ* ones at the *** $p < 0.001$, ** $p < 0.05$, or * $p < 0.09$ level according to a two-tailed Student's *t* test. Similar complementation of the *xrn1Δ* phenotypes is observed in the centromeric and multicopy cRat1 strains. Experiments were repeated three times and averaged. The actual values for the WT (YCpLac33) were 80 ± 9 min for GT, 65 ± 2 fL for cell volume, and 59 ± 6 min for poly(A) mRNA stability. (b) The synthesis rates for all the RNA pol II genes (in arbitrary units, a.u.) were calculated by Genomic Run-on (GRO), as described in the Section 2. The distribution of all the values and their medians is shown in the box and whiskers representation. All the comparisons are significant at the *** $p < 0.001$ level using a Wilcoxon test to compare differences between medians. (c, d) Changes in the synthesis rates (SR) and mRNA half-lives (HL) in an *xrn1Δ* with regard to a WT versus changes caused by adding the cRat1 protein in an *xrn1Δ* background. The high correlation (Pearson, *r*) and the negative slope indicate that the compensation introduced by cRat1 is proportional to the defect caused by the absence of Xrn1. This is especially clear in the SRs. The lower correlation observed in the HL is probably caused by the bigger experimental error associated with their calculation (see the discussion in García-Martínez et al., 2004).

ATGC-3′ and RAT1-R: 5′-TCCTTTTCAAGACGGTGTTTCT-3′, while exogenous *cRAT1* mRNA levels were determined with primers cRAT1-F: 5′-GCAAGGAAGAAATTGATGATGC-3′ and cRAT1-R: 5′-CTGATTCCGCTTTCTCTGTATTTA-3′. Endogenous *ACT1* mRNA levels were utilized for normalization with primers ACT1-F: 5′-TCGTTCCAATTTACGCTGGTT-3′ and ACT1-R: 5′-CGGCCAAATCGATTCTCAA-3′. At least three biological replicates of each sample were analyzed.

2.3 | GRO

GRO was performed as described in (García-Martínez et al., 2004) and as modified in (Oliete-Calvo et al., 2018). Briefly, by macroarray hybridization, GRO detects genome-wide, active elongating RNA polymerase (RNA pol) II, whose density per gene is taken as a measurement of its synthesis rate. At the same time, the protocol allows the mRNA amounts for all the genes to be measured. mRNA half-lives are calculated as the mRNA amount/synthesis rate by assuming steady-state conditions for the transcriptome. The total synthesis rate for a given yeast strain is calculated as the sum of the individual gene synthesis rates. GRO data sets are available at the Gene Expression Omnibus (GEO) with accession numbers: GSE29519 and GSE198240 (reviewer access code: mbyjqgschrcfhib).

2.4 | mRNA half-life calculations

To determine single gene mRNA half-lives, transcriptional shut-off was used following the addition of thiolutin to 5 μg/mL. Samples were collected at 0, 5, 12, 25, 45, 60, and 90 min after thiolutin addition. Samples were analyzed by northern blot analysis using the specific ^{32}P-probes described elsewhere (Pelechano & Pérez-Ortín, 2008).

To determine the general mRNA half-life, a dot-blot strategy was followed as described in García-Martínez et al. (2016). Known amounts of total RNA were spotted onto a nylon membrane and hybridized with a ^{32}P-terminal-labeled oligo d(T)$_{40}$ probe. RNA samples were collected after thiolutin addition at the same times as described for the individual mRNAs. The detailed protocol is described in Benet et al. (2017).

2.5 | HT-5Pseq and 5′Capseq protocols

HT-5PSeq is a method that measures the in vivo presence of 5′P mRNA degradation intermediates in the cell. Thus, unlike ribosome profiling, it focuses on the study of the mRNAs undergoing decay. The HT-5Pseq libraries were prepared as previously reported (Zhang & Pelechano, 2021). Briefly, 6 μg of the DNA-free total RNA were directly ligated with the RNA/RNA oligo containing UMI (RNA rP5_RND oligo). The ligated RNA was reverse-transcribed and primed with the Illumina PE2 compatible oligos containing random hexamers

and oligo-dT. The RNA in the RNA/DNA hybrid was depleted by sodium hydroxide by means of 20 min incubation at 65°C. Ribosomal RNAs were depleted using duplex-specific nuclease with the mixture of ribosomal DNA probes. Samples were amplified by PCR and sequenced in an Illumina NextSeq. 500 instrument employing 60 sequencing cycles for read1 and 15 cycles for read 2.

For the 5′Capseq, the 5′capped mRNAs were captured as previously described (Pelechano et al., 2016). Specifically, 10 μg of total RNA were treated with calf intestinal alkaline phosphatase (NEB) to remove 5′P molecules (fragmented and noncapped). After purification, the mRNA 5′-caps were removed by Cap-Clip (Biozyme), which resulted in 5′P molecules from the previously capped molecules. The following steps were the same as those described for HT-5Pseq (see above), with variations only to skip ribosomal RNA removal. Data sets are available from the GEO database: GSE119114 for the 5Cap-seq data and GSE193992 (reviewer access code: ahadwoocjrivtot) for the HT-5Pseq data.

2.6 | Protein expression levels measurement by western blot analysis

To check for protein expression levels, yeast cells were transformed with the corresponding plasmids and grown as specified in a previous section. Two optical density (OD) units were harvested by centrifugation. Total proteins were extracted from the equivalent number of cells and loaded in sodium dodecyl sulfate polyacrylamide gel electrophoresis to be separated according to their molecular weight. Next, samples were immunoblotted on a nitrocellulose membrane for 90 min at 100 V on ice, as previously described (Ishikawa et al., 1997). Antibodies against FLAG (Sigma-Aldrich), PGK (Invitrogen), and Xrn1 (a gift from A. Johnson) were used. Detection of proteins was performed with an Amersham Imager 600.

2.7 | Bioinformatics procedures

HT-5Pseq reads were trimmed with a 3′-sequencing adapter using *cutadapt* V1.16 (http://gensoft.pasteur.fr/docs/cutadapt/1.6/index.html). The 8 nt random barcodes on the 5′-ends of reads were extracted and added to the header of the *fastq* file as the UMI employing *UMI-tools*. 5′P reads were mapped to *S. cerevisiae* (SGD R64-1-1) using *STAR 2.7.0* with parameter *--alignEndsType Extend5pOfRead1* to exclude soft-clipped bases on the 5′-end. After removing PCR duplications with UMI-tools, an analysis of the 5′-ends positions was performed with the *Fivepseq* package (Nersisyan et al., 2020, http://pelechanolab.com/software/fivepseq), including the relative distance to the start and stop codons. In particular, the unique 5′-mRNA reads in the biological samples were summed and subsequently normalized to reads per million (rpm). Standalone normalized average density plots around genomic features were calculated with the R and Python software *ngs.plot* v2.61 (Shen et al., 2014) using indexed alignment files as inputs and the internal

SacCer3 database annotation as a reference. The statistical robustness parameter, which filters out 0.5% of the genes with the most extreme (high and low) count values, was applied to all the calculations. The 5′Cap reads were processed as described for the HT-5Pseq reads. In general, the 5′Cap reads were trimmed using a 3′-sequencing adapter and the extracted 8 nt random barcodes were employed as UMI. The 5′Cap reads were mapped to *S. cerevisiae* (SGD R64-1-1) with STAR 2.7.0. PCR duplicates were removed by UMI-tools.

Heatmaps and the accompanying average metaplots displaying HT-5Pseq alongside the 5′Capseq data sets were generated by the *bamCoverage*, *computeMatrix*, and *plotHeatmap* functions from the deepTools2 package (Ramírez et al., 2016). The transcription start site (TSS) and the polyA site annotations were taken from Xu et al. (2009). Spearman correlation values and statistical test result asterisks were inserted into the *ggplot2*-generated plots using the *ggpubr* package (https://rpkgs.datanovia.com/ggpubr).

2.8 | Sequence alignment and structural comparison of the Xrn1–ribosome complex and the predicted cRat1–ribosome complex

The Xrn1 (UniProtKB P22147) and cRat1 (UniProtKB Q02792) protein sequences were generally aligned with the Smith and Waterman algorithm (Smith & Waterman, 1981) using the *Jalview* software (Waterhouse et al., 2009).

The *AlphaFold* (Jumper et al., 2021) structure of cRat1 was structurally aligned with *ChimeraX* (Goddard et al., 2018) on the PDB structure 6Q8Y (Tesina et al., 2019). The residues interacting with mRNA and the ribosome were defined as the residues with a least an atom closer than 5 Å to mRNA or other ribosomal subunits. The root mean square deviation per residue was also calculated with ChimeraX. Coloration of the conservation of residues was performed with *ChimeraX* after adapting the *Consurf* palette (Ashkenazy et al., 2016).

3 | RESULTS

3.1 | Cytoplasmic Rat1 partially replaces Xrn1 in the general phenotypes

The Rat1 derivative lacking the NLS (cRat1), which mislocalizes to the cytoplasm, complements some of the cytoplasmic functions of Xrn1, including the defective growth phenotype of the *xrn1Δ* strain (Blasco-Moreno et al., 2019; Johnson, 1997), growth in the presence of benomyl (Johnson, 1997), and the stability of some viral mRNAs (Blasco-Moreno et al., 2019). The present study investigated whether cRat1 complemented the general physiological phenotypes of the *xrn1Δ* strain, including the cell volume, the proliferation rate, and mRNA stabilities. We transformed the wild-type (WT) and *xrn1Δ* strains with a centromeric plasmid containing the cRat1 gene (pBBM3) using an empty vector (YCpLac33) as a control. Although

an xrn1Δ strain expressing Xrn1 from a centromeric plasmid could have been used as a control, we did not expect big differences in expression between the chromosomal and YCp-inserted gene copies (Pérez-Ortín et al., 1987). However, we note that the expression of Xrn1 from the chromosome and a plasmid might not be identical. It should be noted that the WT strain expressing cRat1 also expressed the endogenous WT (including the NLS) nuclear Rat1 version (Blasco-Moreno et al., 2019). In this study, these yeast strains are referred to as cRat1 and WT + cRat1 for simplification reasons (Supporting Information S3: Table S1). Using this series of four strains, we analyzed global poly(A) mRNA stability by transcription shutoff with thiolutin and dot-blot hybridization of the time-course samples. We found that cRat1 reversed most of the global increase in mRNA stability caused by Xrn1 depletion (1.38× vs. 2.43×, regarding the WT taken as 1×; Figure 1a). The addition of cRat1 to a WT strain with natural Xrn1 in the cytoplasm did not alter poly(A) decay (0.98×), which suggests a minor role for cRat1 in mRNA decay when endogenous Xrn1 is also present. Finally, cRat1 mostly restored the GT (1.22×) and cell size (1.07×) of the WT (taken as 1×, Figure 1a).

To verify cRat1 expression, we constructed and analyzed a new series of four strains in which the cRat1 protein had a 3×FLAG epitope at its C-terminal part, and validated its expression by western blot analysis in yeast cells (Supporting Information S1: Figure S1A). The 3×FLAG epitope was necessary for detecting the cRat1 expression because the 1×FLAG version was not sensitive enough (Supporting Information S1: Figure S1A), but it partially affected the strain proliferation rate (Supporting Information S1: Figure S1D). cRat1 without the FLAG epitope, but expressed from the same construct (see Supporting Information S3: Table S1) as that strain, grew similarly to the WT (Supporting Information S1: Figure S1D). Next we measured the mRNA half-lives for two individual mRNAs with medium (*RPL25*) and high (*ACT1*) mRNA stability in an *xrn1Δ* strain, and found that cRat1-3×FLAG restored WT stabilities (Supporting Information S1: Figure S1B). To further assess the effect of cRat1 on mRNA stability, we analyzed global poly(A) decay. This analysis showed that cRat1-3×FLAG partially restored the WT global poly(A) mRNA stabilities (Supporting Information S1: Figure S1C) similarly to the untagged cRat1 version (Figure 1a). Both the GT and cell size were closer to those of the WT, but were not fully recovered (Supporting Information S1: Figure S1C,D), as in the case of the strains without the FLAG epitope (Figure 1a). Interestingly, the noncytoplasmic version of Rat1 with the FLAG epitopes did not rescue the growth defect of the *xrn1Δ* strain (Supporting Information S1: Figure S1D). We conclude that cRat1, with or without the FLAG epitope, behaves similarly in the analyzed phenotypes, but the FLAG epitope has a certain growth detrimental effect. Therefore, although the actual cell volumes, mRNA global stabilities and GTs for both sets of four strains (Figure 1 and Supporting Information S1: Figure S1) were not quantitatively identical, they qualitatively confirmed that cRat1 partially restored the general phenotypes in an *xrn1Δ* background.

Endogenous mRNA and proteins levels for Xrn1 are three to five times higher than for Rat1 (SGD *Saccharomyces* genome

database, 2024). To rule out that the expression level of cRat1 from a centromeric (single-copy per cell plasmid) was too low to fully complement the general physiological phenotypes of an *xrn1Δ* strain, we also tested the expression from a multicopy episomal plasmid (pRS426, see Supporting Information S3: Table S1). As depicted in Figure 1a and Supporting Information S1: Figure S1, the observed phenotypes of the transformed *xrn1Δ* strain with multicopy pRScRAT1 were almost identical to that of those of pBBM3 despite being much highly expressed. This suggests that the phenotypical differences between the WT (*XRN1*) and cRat1 strains are not due to a limiting amount of the cytoplasmic version of the Rat1 protein.

As the cells lacking Xrn1 displayed marked global downregulation of RNA pol II-based transcriptional activity (Haimovich et al., 2013), we next examined whether cRat1 would mitigate the effects on the global RNA pol II synthesis rates. By means of GRO, we found that the mRNA synthesis rate in *xrn1Δ* was 0.36× that of the WT, whereas addition of cRat1 partially compensated for this drop (0.63×, Figure 1b). This partial compensation suggests that the drop in the RNA pol II synthesis rates in the *xrn1Δ* mutants was due not only to the absence of Xrn1 as a transcription activator (Medina et al., 2014), but also to the indirect effect of its lower growth rate on synthesis rates (García-Martínez et al., 2016). Alternatively, or in addition, it is possible that $5' \rightarrow 3'$ mRNA decay per se is important for transcription. Interestingly, the global synthesis rates slightly, but significantly, increased when cRat1 was added to a WT strain (1.15×, Figure 1b) without having any noticeable effect on global mRNA stabilities (Figure 1a).

The compensation in the mRNA synthesis rates and stabilities in a cRat1 strain showed a strong bias in the individual mRNA synthesis rates and stabilities plot: the more affected mRNAs in either synthesis rates or stabilities in *xrn1Δ* were more compensated after adding cRat1 (Figure 1c,d). However, the analysis of the transcriptome-wide differential expression in *xrn1Δ* and the WT strains supplemented with cRat1 did not show any strong biases in either the synthesis rates or mRNA stabilities toward specific gene categories (Supporting Information S4: Table S2). This indicates that cRat1 does not have a significant bias to the $5' \rightarrow 3'$ decay of the mRNAs of the genes belonging to the functional groups, but its effects are mostly related to the actual synthesis and decay rates of mRNAs.

3.2 | Cytoplasmic Rat1 can function cotranslationally in mRNA $5' \rightarrow 3'$ exonuclease, albeit inefficiently

A distinctive function of Xrn1 is to degrade decapped mRNA during its last round of translation (Pelechano et al., 2015). This helps to terminate translation and contributes to the half-lives of many mRNAs (see the Introduction). We next investigated whether cRat1 could perform ribosome-associated co-translational decay. To this end, we measured the presence of 5′-phosphate-containing mRNAs genome wide by 5′P degradome RNA sequencing (HT-5Pseq) in both

sets of four strains: (a) the set of strains transformed with a plasmid containing the Rat1-ΔNLS version (cRat1) without FLAG epitopes or with the empty vector (Figure 2); (b) the set of strains (WT and *xrn1Δ*) transformed, or not, with cRat1-3×FLAG (Supporting Information S1: Figure S2). We used the FLAG tagged cRat1 to check the expression levels in the studied strains (Supporting Information S1: Figure S1A), but we employed the untagged strains for the main experiments to make sure that the Rat1 function was not compromised. Both strain sets provided, however, similar results, which reinforces the reached conclusions (see below).

The WT HT-5Pseq metagene profile was characterized by a 3-nucleotide periodicity pattern and a prominent peak of the HT-5Pseq reads at -17 nt from the STOP codon (Pelechano et al., 2015). HT-5Pseq measures the distance between the $5' \rightarrow 3'$ exonuclease and the trailing ribosome during cotranslational mRNA decay. We have previously shown that the distance between the 5′P of the mRNA undergoing degradation and the first base of the termination codon is 17 nt at the A site of the trailing ribosome (Pelechano et al., 2015; Zhang & Pelechano, 2021). This distance reflects the steric protection offered by the ribosome to the in vivo trimming action of Xrn1p. Unlike the WT, the -17 nt peak was completely lost in *xrn1Δ* and also the reads in 5′-untranslated region (UTR) accumulated in the zone immediately upstream of the AUG codon (blue profiles in Figure 2a, left and right panels). cRat1 partially restored the WT metagene profile to show intermediate levels for the 5′-upstream and -17 nt peaks (light green profile in Figure 2a, left and right panels, respectively). To evaluate genuine ribosome occupancy, we determined the extent of protection from 5′ to 3′ decay in the coding frame in relation to the other two frames. This ratio, known as the "Frame Protection Index" (FPI) (Pelechano et al., 2015; see the Section 2), measures the effectiveness of single-nucleotide coupling between nuclease activity and the ribosome position. As expected, the FPI was compromised in the *xrn1Δ* cells (Figure 2b). The expression of cRat1 in the *xrn1Δ* cells only partially recovered the FPI (increasing from 0.79 in *xrn1Δ* to 0.82 in cRat1, compared to a value of 1 for the WT FPI; see Figure 2b). This finding suggests that Rat1 is somewhat inefficient following the ribosome during co-translational mRNA decay when placed in the cytoplasm.

Given that the HT-5Pseq reads accumulate at the 3′ (close to the STOP codon) in the WT cells and shift to 5′ (close to the AUG codon) in *xrn1Δ*, we reasoned that the proportion of reads in these two regions could serve as a proxy for the efficiency of the $5' \rightarrow 3'$ decay level once degradation had started, taken as either a genome-wide average or a per-gene index. To calculate this 3′ versus 5′ proportion for the WT, *xrn1Δ* and cRat1 strains, we first made low-resolution metagene profiles by spanning the entire gene body (Figure 2c), and then compared the number of reads in the last 20% versus the first 20% of the average gene body region (shadowed areas in Figure 2c). Thus, whereas FPI reflects single-nucleotide coupling between cotranslational decay and the ribosome position along the coding region, the 3′/5′ index denotes the efficiency of $5' \rightarrow 3'$ exonuclease activity and ribosome protection on mRNA. The 3′/5′ index is influenced mainly by translation initiation and termination, which are
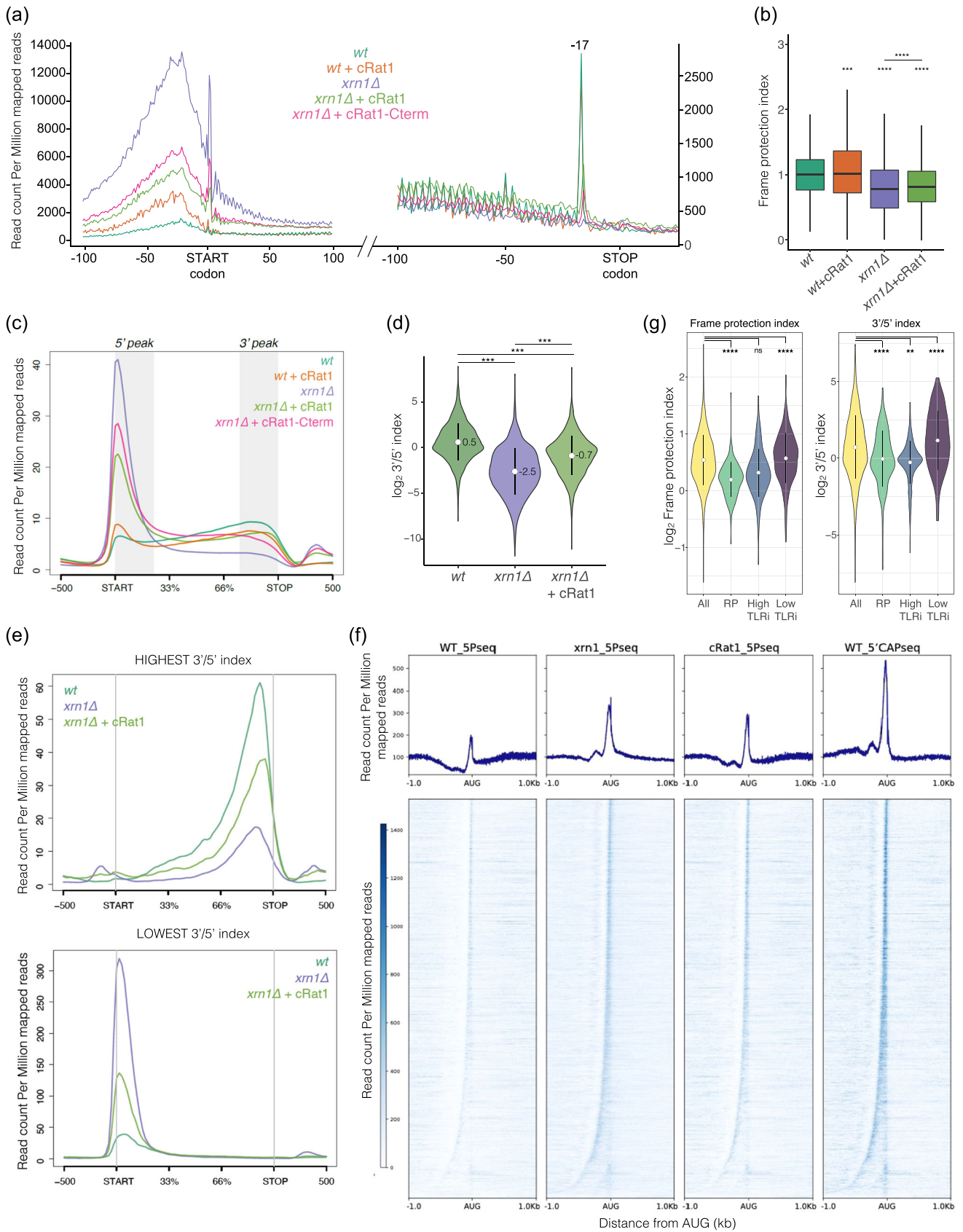
FIGURE 2. (See caption on next page).

the two regions where ribosomes tend to pause the most. As pausing at the stop codon lasts longer in the WT than pausing at the start codon, the general 3′/5′ ratio is expected to be higher than 1. A slow 5′ → 3′ decay results in a 3′/5′ index below 1 (the negative $\log_2$ ratio in Figure 2d). Nevertheless, translation machinery can also protect mRNA from 5′ → 3′ decay, perhaps because the cap is protected (e.g., by eIF4F).

These 3′/5′ indices showed that expressing cRat1 in *xrn1Δ* recovered about 65% of the WT in the 5′ → 3′ decay efficiency lost in *xrn1Δ* (Figure 2d). This result indicates that cRat1 is quite efficient in global 5′ → 3′ degradation (Figure 2b), unlike its poor activity in the pursuit of the last elongating ribosome (FPI value). We next used the per-gene 3′/5′ indices to investigate whether sets of functionally related genes were skewed toward any end of the range. Grouping the 250 genes with the highest values in the 3′/5′ index and the genes with the lowest values revealed that the distributions were similarly skewed in the WT and *xrn1Δ*, but with higher 5′, and lower 3′ peaks for the mutant. The cRat1 sample displayed intermediate behavior (Figure 2e). Therefore, the complementation of the 3′/5′ index made by cRat1 was not biased, but similarly affected all the genes. To confirm this, we next generated metagene plots for specific gene sets. We observed that while the overall shapes of profiles slightly differed for various groups, the proportions of the reads between samples remained approximately the same in all four yeast strains (Supporting Information S1: Figure S2B). This result indicates that lack of Xrn1 (*xrn1Δ*) and its substitution for cRat1 have non specific transcriptome-wide effects. The heatmaps of the individual genes ordered by 5′-UTR length (Figure 2f and Supporting Information S1: Figure S3) showed that the average metagene plots (Figure 2a,c) represented uniform behavior, followed by most mRNAs, with two high-intensity regions at the 5, one where most reads were associated with the TSS (see Supporting Information S1: Figure S3) and ordered according to 5′-UTR length, and another

located around the AUG codon, which we have previously described for multiple species (Huch et al., 2023). This distribution was clearly observed in the summary average count metagene plots (top panels in Figure 2f and Supporting Information S1: Figure S3). The TSS peak detected by HT-5Pseq was particularly clear for *xrn1Δ* and slightly less so for cRat1. The position of this peak corresponded to the canonical capped TSS full-length molecules (as measured by 5Capseq, the rightmost lane in Figure 2f and Supporting Information S1: Figure S3). Altogether, these results suggest that in *xrn1Δ* and, to a lesser extent, in cRat1, a large fraction of the 5′P-detected molecules corresponds to decapped full-length mRNAs.

3.3 | Addition of the C-terminus of Xrn1 to cRat1 does not complement the defect in co-translational decay that characterizes the cRat1 function

The inability of cRat1 to fully complement *xrn1Δ* phenotypes, including the turnover of cytoplasmic mRNAs, suggests that cRat1 does not recognize uncapped mRNAs as well as Xrn1 does (Charenton et al., 2017), or it is not localized close enough to the 5′-ends of cytoplasmic mRNAs. In a previous study, we demonstrated that cRat1 was unable to properly regulate the translation of a subset of membrane protein-coding mRNAs, but was able to do so when fused to the C-terminal domain of Xrn1 (Blasco-Moreno et al., 2019). Therefore, we reasoned that the large unstructured domain of Xrn1, which seems necessary for the interaction with the 5′-UTR of these specific mRNAs, might also be necessary to achieve WT global 5′ → 3′ exonuclease activity and cotranslational 5′-decay levels.

Therefore, to investigate the possible function of Xrn1 Cterm, we created a fusion protein, cRat1-Cterm-3×FLAG, and expressed it in an *xrn1Δ* background. Protein levels were slightly lower than those of regular cRat1-3×FLAG, probably due to a much larger fusion protein

---

FIGURE 2 The cytoplasmic version of the Rat1 protein (cRat1) partially restores the wild-type (WT) HT-5Pseq profile in an *xrnΔ1* strain. The C-terminal region of Xrn1 does not improve cRat1 performance. (a) The HT-5Pseq high-resolution plots showing the profiles of the WT and *xrn1Δ* strains transformed with the empty YCpLac33 plasmid or its version (pBBM3), including the truncated cytoplasmic version of Rat1 (cRat1) without the nuclear localization sequence (NLS) or the same construct fused to the C-terminal domain of Xrn1 (cRat1-Cterm). The metagene analysis for the 5′-monophosphate (5′P) read coverage in relation to the open reading frame (ORF) start (left) and stop codons (right) appears in the samples described above. -17 indicates the position of the characteristic peak produced by the steric protection offered by the ribosome at the stop codon. Three biological replicates of each experiment were merged for every sample. (b) The relative Frame Protection Index (FPI) of the four strains analyzed in (a). The median FPI for the WT was taken as 1. (c) Average gene body metagene plots of the normalized HT-5Pseq read counts around the protein-coding genes. The gene body read coverage is represented as a percentage of the total length of the ORF, whereas the flanking regions around the START and STOP codons represent the real distances from the reference points (represented as base pair length). The shadowed vertical areas highlight the 20% length of both the transcribed region ends used for the calculation of the 3′/5′ index. The gene body-spanning metagene plots were generated using the default curve smoothing implemented in *ngs. plot* with the whole sequencing read. This contrasts to the plots from panel a, generated using the Fivepseq package, where only the most 5′-nucleotide was employed. This explains the apparent different position of the 5′-peak in both panels. (d) Violin plot of the $\log_2$ 3′/5′ index values for the WT, *xrn1Δ*, and cRat1 strains. The added numbers show the median values for each sample. (e) Average metagene plots of the 250 genes with the highest 3′/5′ index values (top panel) or the 250 genes with the lowest (bottom panel) in the WT. (f) Heatmaps of the HT-5Pseq and 5′Capseq data for all the individual protein-coding genes aligned by their START codon and ordered, from top to bottom, by increasing 5′-untranslated region (UTR) length. The corresponding summary average count metagene plots are shown at the top of each heatmap. (g) Violin plots of the $\log_2$ FPI (left) or the 3′/5′ index (right) values in the WT for all the protein-coding genes, ribosomal proteins (RPs), and genes with high or low individual translation rates (TLRi; as described in Forés-Martos et al., 2021). The significance of the median comparisons in panels b, d, and g was estimated using a Wilcoxon test: ns = $p > 0.05$; *$p < 0.05$; **$p < 0.01$; ***$p < 0.001$; ****$p < 0.0001$.

size (Supporting Information S1: Figure S4A). These lower levels did not, however, impede the complementation phenotype that we previously found (Blasco-Moreno et al., 2019). It is important to note that the FLAG epitope, which is carried by cRat1-Cterm, had no noticeable effect on the $5' \rightarrow 3'$ exonuclease activity of cRat1 (see Figure 2 and Supporting Information S1: Figure S2). Both the cell growth and cotranslational decay defects of xrn1Δ were compensated only partially by cRat1-Cterm and to a similar extent to that by regular cRat1 (see the cRat1-Cterm profiles in Figure 2a,c). This finding suggests that Xrn1 performs specific functions that cannot be replaced with Rat1, not even when their main structural difference is minimized using a Rat1-Xrn1-Cterm chimera.

3.4 | *AlphaFold* prediction of the cRat1–ribosome complex suggests poor efficiency for cRat1 during cotranslational mRNA decay

To rationalize the partial functional overlap between cRat1 and Xrn1, we analyzed their sequence and structure conservation. The two proteins showed 30% sequence identity that was, however, not uniformly distributed over protein length. cRat1 aligned only with the first 912 residues of Xrn1, as previously pointed out by Nagarajan et al. (2013) (Figure 3a). Here we further extended this analysis and found that conservation was unevenly distributed with short highly conserved regions (mainly localized in the first half of the protein) spaced by more variable stretches (Figure 3a,b). To understand the role of the conserved regions, we utilized the *AlphaFold* (AF) predicted model of cRat1. The model revealed a structured catalytical domain modeled with good accuracy and two mainly disordered domains with a low *Alphafold Lddt* score (in yellow and orange in Figure 3c). We superimposed the cRat1 model on the Xrn1 chain of the experimentally determined 80S ribosome Xrn1 complex (PDB ID: 6Q8Y). Mapping the sequence conservation on the cRat1 AF model superimposed on Xrn1 revealed significant conservation within the region binding mRNA (Figure 3b,d). Indeed while the overall sequence identity between the two proteins was 30%, the identity of the residues binding mRNA reached 72%. Conversely, only 11% of the residues involved in the Xrn1–ribosome interaction were identical (as depicted in Figure 3a). Even upon closer inspection (Figure 3e), structural similarities between the cRat1 model and the Xrn1 structure in the area of Xrn1 that interacted with the rest of the ribosome were observed, albeit limited to the lower part of the protein. Reassuringly, our predicted cRat1 model is in agreement with experimentally determined published during the revision process of this manuscript (Zeng et al., 2024).

Based on these observations, we can conclude that the high conservation of the mRNA binding/catalytic domain between the two proteins implies that cRat1 likely maintains functional aspects of Xrn1. However, the poor conservation among the residues interacting with the ribosome suggests that cRat1's efficiency in binding to the ribosome-mRNA complex might be poor.
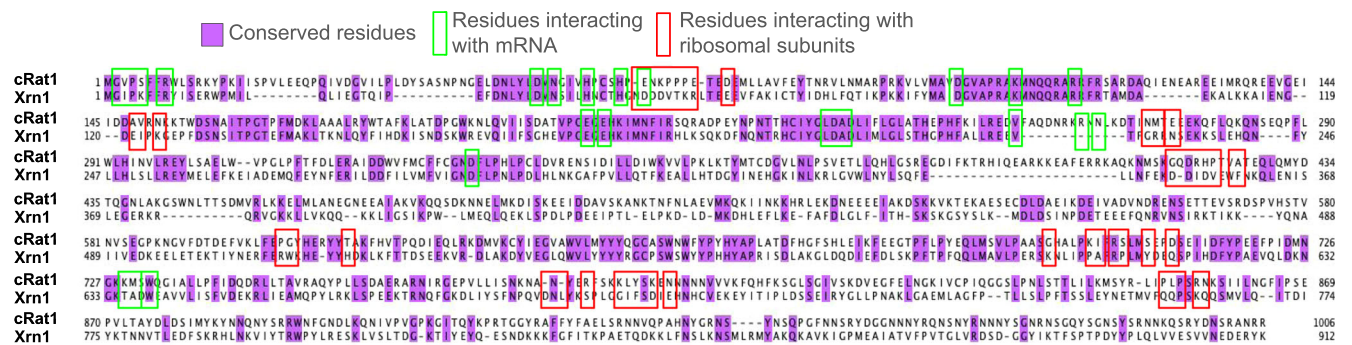
4 | DISCUSSION

A widespread phenomenon during evolution is the accumulation of gene paralogs, for which an interesting question remains to be fully elucidated: do they serve as backups or has each paralog acquired a unique function? Here we focus on two paralogs: Rat1 functions mainly, if not exclusively, in the nucleus, whereas Xrn1 shuttles between the nucleus and the cytoplasm, and accumulates in the cytoplasm. It has been proposed that the two paralogs are fully replaceable and their distinct functions are attributed to their cellular localization (Johnson, 1997). However, the differential activity of these two paralogs has not been fully investigated in the same cellular compartment.

To this end, we investigated whether the cytoplasmic function of Xrn1 could be performed by its nuclear counterpart Rat1. We found that a cytoplasmic version of Rat1 (cRat1) could only partially complement the $5' \rightarrow 3'$ exonuclease activity of the missing Xrn1 in the cytoplasm. cRat1 performance could not be improved, not even when fusing the Xrn1 CTD to the C-terminus of cRat1 (cRat1-Cterm). We further discovered that cRat1 was able to mostly compensate general phenotypes, except for cotranslational mRNA decay. We have evidence that the observed partial complementation was not caused by the lower expression level of cRat1 because when we used a strain that expressed cRat1 in multicopy plasmid (about a 50-fold higher expression level, see Figure 1a and Supporting Information S1: Figure S1), we obtained a similar complementation phenotype. This suggests that the main phenotype was not driven by differential protein abundance but by protein sequence/structure.
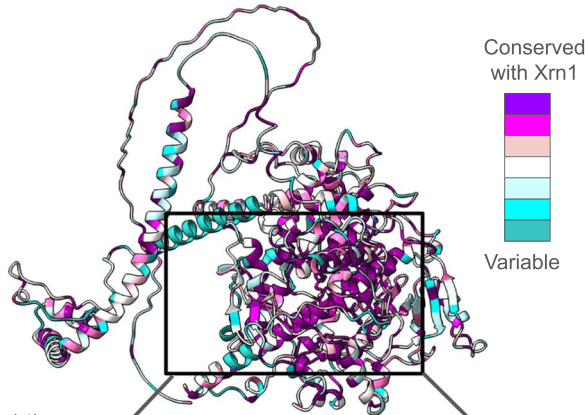
Although cRat1 was able to restore the xrn1Δ defects in cell volume (87%, Figure 1a), the GT (50%, Figure 1a), mRNA stability (73%, Figure 1a), the RNA pol II global synthesis rate (42%, Figure 1b), and even the $3'/5'$ index (74%, Figure 2d), it was much less efficient in compensating the effects on the co-translational mRNA decay rates (13%, Figure 2b, see below). The partial recovery in the synthesis rate could be attributed to indirect effects. We previously found that XRN1 deletion resulted in defective transcription, which was attributed to both direct and indirect effects (Chattopadhyay et al., 2022; Haimovich et al., 2013; Medina et al., 2014). Direct effects could be the result of loss of the direct function of Xrn1 during transcription activation (Haimovich et al., 2013), whereas indirect effects were probably the consequence of the strain's slow growth. Given the observation that cRat1 partially recovered the growth defect of the xrn1Δ cells, the cRat1-mediated increase in transcription of these xrn1Δ cells could be due to the compensation in the growth rate given the close relation between the RNA pol II synthesis rates and growth rates (García-Martínez et al., 2016). This leaves co-translational decay as the activity of Xrn1 that is the worst complemented by cRat1.

Interestingly, cRat1 could slightly, but significantly, increase transcription in WT cells. We hypothesized that cRat1 could compete with Xrn1 for binding substrates. This possible competition would possibly provide a plausible explanation for this transcriptional increase in WT cells because cRat1 could increase
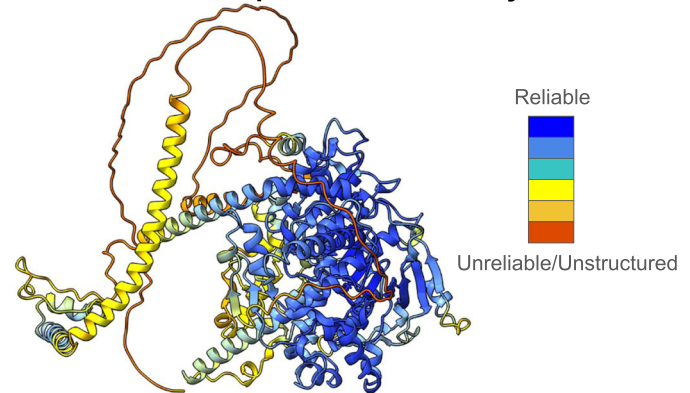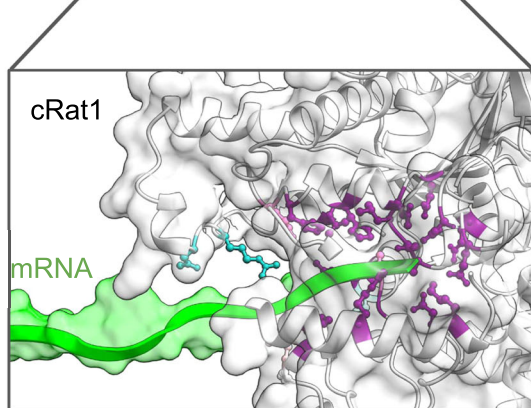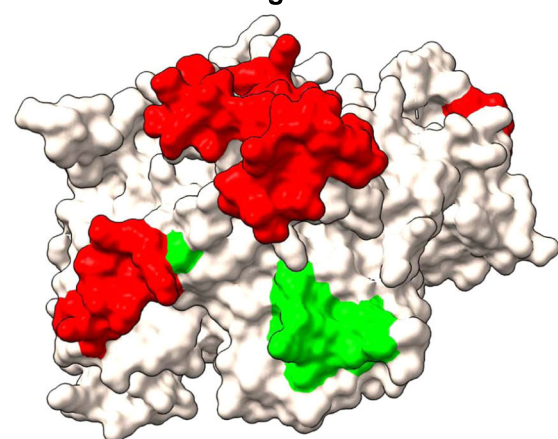
FIGURE 3. The sequence alignment and structural superposition between cRat1 and Xrn1 highlight the conserved catalytic site. (a) Sequence alignment between cRat1 and Xrn1. Identical residues are colored in purple. Green boxes highlight the residues that bind messenger RNA (mRNA). Red boxes highlight the residues that interact with ribosomal subunits. (b) The sequence conservation between cRat1 and Xrn1 mapped on the cRat1 model. The residues conservation between the two proteins is shown with the color scale on the right. Identical residues are colored purple. Similar residues are shown in pink shades. The more divergent residues substitutions and insertions are highlighted with blue shades. Conservation is calculated based on the alignment of panel a. (c) The panel shows the *AlphaFold* model for cRat1. Its coloration corresponds to the reliability of the structural prediction according to the *AlphaFold* database: reliable regions are colored in blue shades, while less reliable and unstructured regions are colored in yellow and red, respectively. (d) The zoom of the catalytic region of the cRat1 *AlphaFold* model (in white) and mRNA (in green). The residues of cRat1 that interact with mRNA are colored according to their conservation with Xrn1. (e) The surface of the *AlphaFold* model for cRat1 is superimposed on the Xrn1 structure. cRat1 residues 400–589 and 879–1006 are hidden for clarity, because they are unreliable/unstructured according to *AlphaFold*. The cRat1 surface is colored in white, but the regions of cRat1 correspondent to the areas of Xrn1 that interact with the PDB structure that, in turn, interacts with the ribosomal subunits are highlighted in red and green. Red depicts the structures that do not overlap and green represents those that overlap between the backbone of cRat1, and Xrn1 is closer than 1 Å of root mean square deviation (RMSD) per residue.

the amount of free Xrn1, capable of being imported to the nucleus to activate transcription. It is also possible that mRNA decay per se may enhance transcription (e.g., by supplying more nucleotides).

It would seem that, in the absence of XRN1, cRat1 could provide some mRNA buffering activity (Figure 1a). Hence, partial mRNA buffering could apparently be accomplished without both Xrn1 and its specific shuttling feature. Interestingly, we found that the compensation introduced by cRat1 was proportional to the defect caused by the absence of Xrn1 (Figure 1c,d). Perhaps the observation that the decapping rate was one of the limiting activities during mRNA decay (Parker, 2012) would be relevant for this correlation. We propose that mRNA degradation per se can provide some buffering, probably together with other pathways and partners that act in concert or in parallel. In particular, our results suggest that the transcription activation capacity of Xrn1 is not absolutely required for buffering (assuming that cRat1 does not possess this function). However, seeing that this buffering is partial, it is clear that mRNA decay is not sufficient to provide full buffering. Maybe transcription activation and the specific shuttling features of Xrn1 are required for efficient buffering.

As previously pointed out, the effect of cRat1 expression on the start of $5' \rightarrow 3'$ mRNA decay after decapping (the HT-5Pseq profiles and the $3'/5'$ index) of the $xrn1\Delta$ cells was quite low. Using heatmaps of HT-5Pseq data, we noticed that the accumulation of decapped, but not $5' \rightarrow 3'$ trimmed, mRNAs (i.e., overlapping the TSS sites) was intermediate between the WT strain and the $xrn1\Delta$ cells (Figure 2f and Supporting Information S1: Figure S3). This suggests that cRat1 is not as efficient as Xrn1 in targeting decapped 5′P mRNA molecules. Thus when measuring a snapshot of the mRNAs that underwent degradation, the 5′P molecules that overlapped TSS transiently accumulated in the cRat1 strain. Although we attempted to control for all the external factors whenever possible, we could not rule out that some of the observed differences between strains could also be influenced by differences in ribosome dynamics (e.g., velocity of ribosome or ribosome drop-off rates). Regarding the degradation inside the ORF, the 3 nt degradation pattern in an $xrn1\Delta$ was lost. When taking the FPI value of the $xrn1\Delta$ mutant that lacked cytoplasmic $5' \rightarrow 3'$ XRN as a bottom reference (0.79) and the WT value as 1, we observed that the cRat1 strain only increased the FPI value by 13% (up to 0.82). This indicates that cRat1 is not a good substitute for Xrn1 for following the ribosome position during cotranslational mRNA decay. What this means is that although cRat1 is capable of degrading 5′P mRNA molecules, the in vivo kinetics for the exonuclease to find decapped mRNAs and to chase them to the ribosome position is suboptimal. Given that the Cterm of Xrn1 did not improve the cRat1 function, we concluded that the N-terminal two thirds of Xrn1 contained all the determinants needed for $5' \rightarrow 3'$ cotranslational decay as measured by HT-5Pseq. This conclusion is supported by the fact that the Xrn1 interacted with ribosomes via the 1–772 amino acids region and no interaction was detected with its Cterm domain (Tesina et al., 2019). The specific reason why cRat1 is a poor substitute for Xrn1 during co-translational decay remains to be

determined. Our structural comparison of the experimentally determined Xrn1-ribosome complex with the *AlphaFold* prediction of a cRat1–ribosome interaction suggests that the vast majority of the residues in Xrn1 involved in mRNA binding are identical in cRat1. These findings confirm that the $5' \rightarrow 3'$ exonuclease function is conserved and suggest that cRat1 might attack the 5′P-ends of translating mRNAs. However, the structural superposition between the two proteins implies that cRat1 is unable to mimic the Xrn1-ribosome interaction. Thus our model indicates that cRat1 is likely worse than Xrn1 for following the last translating ribosome and performing $5' \rightarrow 3'$ cotranslational decay.

XRN1 and *RAT1* are paralogous genes that do not derive from whole-genome duplication (Wolfe, 2015), but from an older small-scale duplication event (Fares et al., 2013). They show intermediate homology and are present in most eukaryotes from yeast to humans (Parker & Song, 2004), which suggests a long time for sequence divergence. However, they can reciprocally rescue each other's lethal phenotypes in yeast (Johnson, 1997). Here we confirm that their exonuclease activities are partially interchangeable. Interestingly, both exonucleases have evolved to chase after processive synthesis machines: Rat1 pursues RNA pol II as a torpedo and degrades the nascent mRNA in the nucleus (Nagarajan et al., 2013), whereas Xrn1 pursues and degrades decapped mRNA after the last translating ribosome (Pelechano et al., 2015). Nevertheless, it would seem that the specialization of the two $5' \rightarrow 3'$ exonucleases makes them different in terms of the interactive partners that they bind to, perhaps mediated by the presence or absence of Xrn1-Cterm. However, the addition of Xrn1-Cterm to Rat1 does not suffice to make it fully interchangeable with Xrn1. Therefore, it is important to note that their subcellular distribution and dynamics are critical for their differential activities. Rat1 is predominantly nuclear, whereas Xrn1 is largely cytoplasmic (Haimovich et al., 2013; Johnson, 1997; Sharma et al., 2022). Rat1 can substitute for Xrn1 when its NLS is deleted and becomes cytoplasmic (Sharma et al., 2022; this paper), but Xrn1 can only complement the *rat1* mutant when it is overexpressed from a multicopy plasmid and is fused to a strong SV40 large-T-antigen NLS (Johnson, 1997). Moreover, Xrn1 can perform nucleo-cytoplasmic shuttling. Hence the number of nuclear and cytoplasmic $5' \rightarrow 3'$ exonuclease molecules, and the capacity to shuttle, determine the functional difference between these two exonucleases. These features presumably appeared early during eukaryotic evolution and made it impossible to completely substitute one protein for the other despite their similar and partially interchangeable exonuclease activities.

CONFLICT OF INTEREST STATEMENT

Vicent Pelechano is a cofounder and shareholder of 3N Bio AB. All the other authors declare no conflict of interest.

DATA AVAILABILITY STATEMENT

The data supporting our findings are available in the Supporting Information. In addition, genomic data are available at the Gene Expression Omnibus (GEO; https://www.ncbi.nlm.nih.gov/geo/): 5Cap-seq data under accession number GSE119114, HT-5Pseq data under accession number GSE193992, and the GRO data under the accession numbers GSE29519 and GSE198240. The latest version of *Fivepseq* package (http://pelechanolab.com/software/fivepseq/) was used for HT-5Pseq data analysis.

ORCID

José E. Pérez-Ortín 🄳 http://orcid.org/0000-0002-1992-513X
Leire de Campos-Mata 🄳 http://orcid.org/0000-0003-1998-4014

REFERENCES

Amberg, D. C., Goldstein, A. L., & Cole, C. N. (1992). Isolation and characterization of RAT1: An essential gene of *Saccharomyces cerevisiae* required for the efficient nucleocytoplasmic trafficking of mRNA. *Genes & Development*, *6*, 1173–1189. https://doi.org/10.1101/gad.6.7.1173

Ashkenazy, H., Abadi, S., Martz, E., Chay, O., Mayrose, I., Pupko, T., & Ben-Tal, N. (2016). ConSurf 2016: An improved methodology to estimate and visualize evolutionary conservation in macromolecules. *Nucleic Acids Research*, *44*(W1), W344–W350. https://doi.org/10.1093/nar/gkw408

Basu, S., Mallik, S., Hait, S., & Kundu, S. (2021). Genome-scale molecular principles of mRNA half-life regulation in yeast. *The FEBS Journal*, *288*(11), 3428–3447. https://doi.org/10.1111/febs.15670

Benet, M., Miguel, A., Carrasco, F., Li, T., Planells, J., Alepuz, P., Tordera, V., & Pérez-Ortín, J. E. (2017). Modulation of protein synthesis and degradation maintains proteostasis during yeast growth at different temperatures. *Biochimica et Biophysica Acta (BBA) - Gene Regulatory Mechanisms*, *1860*(7), 794–802. https://doi.org/10.1016/j.bbagrm.2017.04.003

Blasco-Moreno, B., de Campos-Mata, L., Böttcher, R., García-Martínez, J., Jungfleisch, J., Nedialkova, D. D., Chattopadhyay, S., Gas, M. E., Oliva, B., Pérez-Ortín, J. E., Leidel, S. A., Choder, M., & Díez, J. (2019). The exonuclease Xrn1 activates transcription and translation of mRNAs encoding membrane proteins. *Nature Communications*, *10*(1), 1298. https://doi.org/10.1038/s41467-019-09199-6

Chang, J. H., Xiang, S., & Tong, L. (2012). Structures of 5′-3′ exoribonucleases. *Enzymes*, *31*, 15–29. https://doi.org/10.1016/B978-0-12-404740-2.00006-9

Chang, J. H., Xiang, S., & Tong, L. (2011). 5′-3′ Exoribonucleases. In: A. W. Nicholson (Ed.), *Ribonucleases* (Vol. 7, pp. 167–192). Springer.

Charenton, C., Gaudon-Plesse, C., Fourati, Z., Taverniti, V., Back, R., Kolesnikova, O., Séraphin, B., & Graille, M. (2017). A unique surface on Pat1 C-terminal domain directly interacts with Dcp2 decapping enzyme and Xrn1 5′-3′ mRNA exonuclease in yeast. *Proceedings of the National Academy of Sciences of the United States of America*, *114*(45), 9493. https://doi.org/10.1073/pnas.1711680114

Chattopadhyay, S., Garcia-Martinez, J., Haimovich, G., Fischer, J., Khwaja, A., Barkai, O., Chuartzman, S. G., Schuldiner, M., Elran, R., Rosenberg, M. I., Urim, S., Deshmukh, S., Bohnsack, K. E., Bohnsack, M. T., Perez-Ortin, J. E., & Choder, M. (2022). RNA-controlled nucleocytoplasmic shuttling of mRNA decay factors regulates mRNA synthesis and a novel mRNA decay pathway. *Nature Communications*, *13*, 7184. https://doi.org/10.1038/s41467-022-34417-z

Christianson, T. W., Sikorski, R. S., Dante, M., Shero, J. H., & Hieter, P. (1992). Multifunctional yeast high-copy-number shuttle vectors. *Gene*, *110*(1), 119–122. https://doi.org/10.1016/0378-1119(92)90454-w

Fares, M. A., Keane, O. M., Toft, C., Carretero-Paulet, L., & Jones, G. W. (2013). The roles of whole-genome and small-scale duplications in the functional specialization of *Saccharomyces cerevisiae* genes. *PLoS Genetics*, *9*, e1003176. https://doi.org/10.1371/journal.pgen.1003176

Forés-Martos, J., Forte, A., García-Martínez, J., & Pérez-Ortín, J. E. (2021). A trans-omics comparison reveals common gene expression strategies in four model organisms and exposes similarities and differences between them. *Cells*, *10*(2), 334. https://doi.org/10.3390/cells10020334

García-Martínez, J., Delgado-Ramos, L., Ayala, G., Pelechano, V., Medina, D. A., Carrasco, F., González, R., Andrés-León, E., Steinmetz, L., Warringer, J., Chávez, S., & Pérez-Ortín, J. E. (2016). The cellular growth rate controls overall mRNA turnover, and modulates either transcription or degradation rates of particular gene regulons. *Nucleic Acids Research*, *44*, 3643–3658. https://doi.org/10.1093/nar/gkv1512

García-Martínez, J., Aranda, A., & Pérez-Ortín, J. E. (2004). Genomic Run-On evaluates transcription rates for all yeast genes and identifies gene regulatory mechanisms. *Molecular Cell*, *15*, 303–313. https://doi.org/10.1016/j.molcel.2004.06.004

Garre, E., Romero-Santacreu, L., Barneo-Muñoz, M., Miguel, A., Pérez-Ortín, J. E., & Alepuz, P. (2013). Nonsense-mediated mRNA decay controls the changes in yeast ribosomal protein pre-mRNAs levels upon osmotic stress. *PLoS One*, *8*(4), e61240. https://doi.org/10.1371/journal.pone.0061240

Gietz, R. D., & Schiestl, R. H. (2007). High-efficiency yeast transformation using the LiAc/SS carrier DNA/PEG method. *Nature Protocols*, *2*(1), 31–34. https://doi.org/10.1038/nprot.2007.13

Goddard, T. D., Huang, C. C., Meng, E. C., Pettersen, E. F., Couch, G. S., Morris, J. H., & Ferrin, T. E. (2018). UCSF ChimeraX: Meeting modern challenges in visualization and analysis. *Protein Science*, *27*(1), 14–25. https://doi.org/10.1002/pro.3235

Haimovich, G., Medina, D. A., Causse, S. Z., Garber, M., Millán-Zambrano, G., Barkai, O., Chávez, S., Pérez-Ortín, J. E., Darzacq, X., & Choder, M. (2013). Gene expression is circular: Factors for mRNA degradation also foster mRNA synthesis. *Cell*, *153*(5), 1000–1011. https://doi.org/10.1016/j.cell.2013.05.012

Han, W. Y., Hou, B. H., Lee, W. C., Chan, T. C., Lin, T. H., & Chen, H. M. (2023). *Arabidopsis* mRNA decay landscape shaped by XRN 5′-3′ exoribonucleases. *The Plant Journal*, *114*, 895–913. https://doi.org/10.1111/tpj.16181

Heyer, W. D., Johnson, A. W., Reinhart, U., & Kolodner, R. D. (1995). Regulation and intracellular localization of *Saccharomyces cerevisiae* strand exchange protein 1 (Sep1/Xrn1/Kem1), a multifunctional exonuclease. *Molecular and Cellular Biology*, *15*, 2728–2736. https://doi.org/10.1128/mcb.15.5.2728

Huch, S., Nersisyan, L., Ropat, M., Barrett, D., Wu, M., Wang, J., Valeriano, V. D., Vardazaryan, N., Huerta-Cepas, J., Wei, W., Du, J., Steinmetz, L. M., Engstrand, L., & Pelechano, V. (2023). Atlas of mRNA translation and decay for bacteria. *Nature Microbiology*, *8*, 1123–1136. https://doi.org/10.1038/s41564-023-01393-z

Interthal, H., Bellocq, C., Bähler, J., Bashkirov, V. I., Edelstein, S., & Heyer, W. D. (1995). A role of Sep1 (=Kem1, Xrn1) as a microtubule-associated protein in *Saccharomyces cerevisiae*. *The EMBO Journal*, *14*(6), 1057–1066. https://doi.org/10.1002/j.1460-2075.1995.tb07088.x

Ishikawa, M., Díez, J., Restrepo-Hartwig, M., & Ahlquist, P. (1997). Yeast mutations in multiple complementation groups inhibit brome mosaic virus RNA replication and transcription and perturb regulated expression of the viral polymerase-like gene. *Proceedings of the National Academy of Sciences*, *94*(25), 13810–13815. https://doi.org/10.1073/pnas.94.25.13810

Johnson, A. W. (1997). Rat1p and Xrn1p are functionally interchangeable exoribonucleases that are restricted to and required in the nucleus and cytoplasm, respectively. *Molecular and Cellular Biology*, *17*(10), 6122–6130. https://doi.org/10.1128/MCB.17.10.6122

Johnson, A. W., & Kolodner, R. D. (1995). Synthetic lethality of sep1 (xrn1) ski2 and sep1 (xrn1) ski3 mutants of *Saccharomyces cerevisiae* is independent of killer virus and suggests a general role for these genes in translation control. *Molecular and Cellular Biology*, *15*(5), 2719–2727. https://doi.org/10.1128/MCB.15.5.2719

Jumper, J., Evans, R., Pritzel, A., Green, T., Figurnov, M., Ronneberger, O., Tunyasuvunakool, K., Bates, R., Žídek, A., Potapenko, A., Bridgland, A., Meyer, C., Kohl, S. A. A., Ballard, A. J., Cowie, A., Romera-Paredes, B., Nikolov, S., Jain, R., Adler, J., ... Hassabis, D. (2021). Highly accurate protein structure prediction with AlphaFold. *Nature*, *596*, 583–589. https://doi.org/10.1038/s41586-021-03819-2

Kenna, M., Stevens, A., McCammon, M., & Douglas, M. G. (1993). An essential yeast gene with homology to the exonuclease-encoding XRN1/KEM1 gene also encodes a protein with exoribonuclease activity. *Molecular and Cellular Biology*, *13*(1), 341–350. https://doi.org/10.1128/mcb.13.1.341-350.1993

Kim, J., Ljungdahl, P. O., & Fink, G. R. (1990). kem mutations affect nuclear fusion in *Saccharomyces cerevisiae*. *Genetics*, *126*(4), 799–812. https://doi.org/10.1093/genetics/126.4.799

Kim, M., Krogan, N. J., Vasiljeva, L., Rando, O. J., Nedea, E., Greenblatt, J. F., & Buratowski, S. (2004). The yeast Rat1 exonuclease promotes transcription termination by RNA polymerase II. *Nature*, *432*(7016), 517–522. https://doi.org/10.1038/nature03041

Langeberg, C. J., Welch, W. R. W., McGuire, J. V., Ashby, A., Jackson, A. D., & Chapman, E. G. (2020). Biochemical characterization of yeast Xrn1. *Biochemistry*, *59*, 1493–1507. https://doi.org/10.1021/acs.biochem.9b01035

Larimer, F. W., Hsu, C. L., Maupin, M. K., & Stevens, A. (1992). Characterization of the XRN1 gene encoding a 5′-->3′ exoribonuclease: Sequence data and analysis of disparate protein and mRNA levels of gene-disrupted yeast cells. *Gene*, *120*(1), 51–57. https://doi.org/10.1016/0378-1119(92)90008-d

Larimer, F. W., & Stevens, A. (1990). Disruption of the gene XRN1, coding for a 5′→3′ exoribonuclease, restricts yeast cell growth. *Gene*, *95*(1), 85–90. https://doi.org/10.1016/0378-1119(90)90417-p

Medina, D. A., Jordán-Pla, A., Millán-Zambrano, G., Chávez, S., Choder, M., & Pérez-Ortín, J. E. (2014). Cytoplasmic 5′-3′ exonuclease Xrn1p is also a genome-wide transcription factor in yeast. *Frontiers in Genetics*, *5*, 1. https://doi.org/10.3389/fgene.2014.00001

Nagarajan, V. K., Jones, C. I., Newbury, S. F., & Green, P. J. (2013). XRN 5′→3′ exoribonucleases: Structure, mechanisms and functions. *Biochimica et Biophysica Acta (BBA) - Gene Regulatory Mechanisms*, *1829*, 590–603. https://doi.org/10.1016/j.bbagrm.2013.03.005

Nersisyan, L., Ropat, M., & Pelechano, V. (2020). Improved computational analysis of ribosome dynamics from 5′P degradome data using fivepseq. *NAR Genomics and Bioinformatics*, *2*(4), lqaa099. https://doi.org/10.1093/nargab/lqaa099

Oliete-Calvo, P., Serrano-Quílez, J., Nuño-Cabanes, C., Pérez-Martínez, M. E., Soares, L. M., Dichtl, B., Buratowski, S., Pérez-Ortín, J. E., & Rodríguez-Navarro, S. (2018). A role for Mog1 in H2Bub1 and H3K4me3 regulation affecting RNAPII transcription and mRNA export. *EMBO Reports*, *19*(11), e45992. https://doi.org/10.15252/embr.201845992

Page, A. M., Davis, K., Molineux, C., Kolodner, R. D., & Johnson, A. W. (1998). Mutational analysis of exoribonuclease I from *Saccharomyces cerevisiae*. *Nucleic Acids Research*, *26*(16), 3707–3716. https://doi.org/10.1093/nar/26.16.3707

Parker, R. (2012). RNA degradation in *Saccharomyces cerevisae*. *Genetics*, *191*(3), 671–702. https://doi.org/10.1534/genetics.111.137265

Parker, R., & Song, H. (2004). The enzymes and control of eukaryotic mRNA turnover. *Nature Structural & Molecular Biology*, *11*(2), 121–127. https://doi.org/10.1038/nsmb724

Pelechano, V., & Pérez-Ortín, J. E. (2008). The transcriptional inhibitor thiolutin blocks mRNA degradation in yeast. *Yeast*, *25*(2), 85–92. https://doi.org/10.1002/yea.1548

Pelechano, V., Wei, W., & Steinmetz, L. M. (2015). Widespread co-translational RNA decay reveals ribosome dynamics. *Cell*, *161*, 1400–1412. https://doi.org/10.1016/j.cell.2015.05.008

Pelechano, V., Wei, W., & Steinmetz, L. M. (2016). Genome-wide quantification of 5′-phosphorylated mRNA degradation intermediates for analysis of ribosome dynamics. *Nature Protocols*, *11*, 359–376. https://doi.org/10.1038/nprot.2016.026

Pérez-Ortín, J. E., & Chávez, S. (2022). Nucleo-cytoplasmic shuttling of RNA-binding factors: mRNA buffering and beyond. *Biochimica et Biophysica Acta (BBA) - Gene Regulatory Mechanisms*, *1865*(5), 194849. https://doi.org/10.1016/j.bbagrm.2022.194849

Pérez-Ortín, J. E., Estruch, F., Matallana, E., & Franco, L. (1987). Fine analysis of the chromatin structure of the yeast SUC2 gene and of its changes upon derepression. Comparison between the chromosomal and plasmid-inserted genes. *Nucleic Acids Research*, *15*(17), 6937–6956. https://doi.org/10.1093/nar/15.17.6937

Ramírez, F., Ryan, D. P., Grüning, B., Bhardwaj, V., Kilpert, F., Richter, A. S., Heyne, S., Dündar, F., & Manke, T. (2016). deepTools2: A next generation web server for deep-sequencing data analysis. *Nucleic Acids Research*, *44*(W1), W160–W165. https://doi.org/10.1093/nar/gkw25

SGD. (2024). *Saccharomyces genome database*. https://www.yeastgenome.org/

Sharma, S., Yang, J., Grudzien-Nogalska, E., Shivas, J., Kwan, K. Y., & Kiledjian, M. (2022). Xrn1 is a deNADding enzyme modulating mitochondrial NAD-capped RNA. *Nature Communications*, *13*(1), 889. https://doi.org/10.1038/s41467-022-28555-7

Shen, L., Shao, N., Liu, X., & Nestler, E. (2014). ngs.plot: Quick mining and visualization of next-generation sequencing data by integrating genomic databases. *BMC Genomics*, *15*:284. https://doi.org/10.1186/1471-2164-15-284

Smith, T. F., & Waterman, M. S. (1981). Identification of common molecular subsequences. *Journal of Molecular Biology*, *147*(1), 195–197. https://doi.org/10.1016/0022-2836(81)90087-5

Solinger, J. A., Pascolini, D., & Heyer, W. D. (1999). Active-site mutations in the Xrn1p exoribonuclease of *Saccharomyces cerevisiae* reveal a specific role in meiosis. *Molecular and Cellular Biology*, *19*(9), 5930–5942. https://doi.org/10.1128/MCB.19.9.5930

Tesina, P., Heckel, E., Cheng, J., Fromont-Racine, M., Buschauer, R., Kater, L., Beatrix, B., Berninghausen, O., Jacquier, A., Becker, T., & Beckmann, R. (2019). Structure of the 80S ribosome-Xrn1 nuclease complex. *Nature Structural & Molecular Biology*, *26*(4), 275–280. https://doi.org/10.1038/s41594-019-0202-5

Waterhouse, A. M., Procter, J. B., Martin, D. M. A., Clamp, M., & Barton, G. J. (2009). Jalview version 2—A multiple sequence alignment editor and analysis workbench. *Bioinformatics*, *25*(9), 1189–1191. https://doi.org/10.1093/bioinformatics/btp033

Wolfe, K. H. (2015). Origin of the yeast whole-genome duplication. *PLoS Biology*, *13*(8), e1002221. https://doi.org/10.1371/journal.pbio.1002221

Xiang, S., Cooper-Morgan, A., Jiao, X., Kiledjian, M., Manley, J. L., & Tong, L. (2009). Structure and function of the 5′→3′ exoribonuclease Rat1 and its activating partner Rai1. *Nature*, *458*(7239), 784–788. https://doi.org/10.1038/nature07731

Xu, Z., Wei, W., Gagneur, J., Perocchi, F., Clauder-Münster, S., Camblong, J., Guffanti, E., Stutz, F., Huber, W., & Steinmetz, L. M. (2009). Bidirectional promoters generate pervasive transcription in yeast. *Nature*, *457*(7232), 1033–1037. https://doi.org/10.1038/nature07728

Zeng Y., Zhang H. W., Wu X. X., Zhang Y. (2024). Structural basis of exoribonuclease-mediated mRNA transcription termination. *Nature*, *628* (8009), 887–893. https://doi.org/10.1038/s41586-024-07240-3

Zhang, Y., & Pelechano, V. (2021). Application of high-throughput 5′P sequencing for the study of co-translational mRNA decay. *STAR Protocols*, *2*(2), 100447. https://doi.org/10.1016/j.xpro.2021.100447

SUPPORTING INFORMATION

Additional supporting information can be found online in the Supporting Information section at the end of this article.